Iodine speciation and size distribution in ambient aerosols at a coastal new particle formation hotspot of China

Huan Yu[1,2], Lili Ren[2], Xiangpeng Huang[2], Mingjie Xie[2], Jun He[3], Hang Xiao[4]

1. Department of Atmospheric Science, School of Environmental Studies, China University of Geosciences, Wuhan 430074, China
2. School of Environmental Science and Engineering, Nanjing University of Information Science and Technology, Nanjing 210044, China
3. Department of Chemical and Environmental Engineering, University of Nottingham Ningbo China, Ningbo 315100, China
4. Ningbo Urban Environment Observation and Research Station, Institute of Urban Environment, Chinese Academy of Sciences, Xiamen 361021, China

Correspondence to: Huan Yu (yuhuan_1981@163.com)

Abstract

Intense new particle formation (NPF) events were observed in the coastal atmosphere during algae growth and farming season at Xiangshan Gulf of east China coast. High nucleation-mode iodine concentrations measured by ultra-performance liquid chromatography coupled with quadrupole time-of-flight mass spectrometry (UPLC/Q-TOF-MS) confirmed that the NPF events were induced by iodine species. Our study provided important information of iodine speciation, size distribution and its role in NPF in the context of heavy air pollution in China’s coastal areas. For the first time, we identified 5 inorganic iodine species, 45 organic iodine compounds (35 molecular formulas) and a group of iodide-organic adducts in aerosols. The concentrations and size distributions of iodine species down to 10 nanometers were measured during the iodine-induced NPF, continental NPF and non-NPF days at the coastal site and compared to those at an inland site. The iodine in the above four types of aerosol samples were characterized by iodate, aromatic iodine compounds, iodoacetic acid/iodopropenoic acid and iodide-organic adducts, respectively. Iodide and organic iodine compounds were found in the nucleation mode particles, however, it is still not clear whether they contributed to nucleation or just new particle growth. Wild algae, as well as farmed algae, could be an important NPF source in China's coastal areas.

1. Introduction

Iodine is an essential trace element for all mammals (including human beings) and some aquatic plants. The atmospheric impact of iodine includes ozone (O_3) depletion, altering HO_x and NO_x chemistry, mercury oxidation and aerosol formation (Baker et al., 2001; O'Dowd et al., 2002). Marine emission sources of iodine containing species in the atmosphere, such as iodomethane, molecular iodine (I_2), hypoiodous acid (HOI) include marine biota emission (Baker et al., 2000), sea surface iodide (I^-) activation by O_3 (Dixneuf et al., 2009; Mcfiggans et al., 2004; Palmer et al., 2005; Sellegri et al., 2006) and sea surface bubble bursting (Seto and Duce, 1972). Continental iodine sources include soil emission, fossil fuel and biomass combustions and industrial emissions (Redeker et al., 2000; Sive et al., 2007). In recent years, much attention has been paid to the new particle formation (NPF) induced by iodine species (Dall'Osto et al., 2018; Allan et al., 2015; Roscoe et al., 2015; Mahajan et al., 2011; McFiggans et al., 2010; O'Dowd and De Leeuw, 2007; Grose et al., 2007; Yoon et al., 2006; O'Dowd et al., 2002). Based upon current knowledge, a simplified scheme of iodine oxidation and nucleation is described as follows: volatile iodocarbons or I_2 photolyse to I atoms, which react with O_3 to produce IO and IO_2 radicals; subsequently the self-combination of IO and IO_2 forms iodine oxides I_2O_{2-5}; iodine oxoacids HIO_x(x=1-3) were produced either from I_2O_{2-5} hydration or via the reaction of IO and IO_2 reaction with HO_x (Burkholder et al., 2004; Mart ń et al., 2013;

Sipilä et al., 2016); eventually, the clustering of I_2O_{2-5} (or HIO_x) and the subsequent growth of these iodine particles in the presence of other condensable vapors contribute to cloud condensation nuclei (CCN) so as to influence the climate.

In the past, iodine concentration or speciation has been measured in natural and drinking water (Chen et al., 2007; Liu et al., 2015; Wang and Jiang, 2008; Wei et al., 2007), precipitation (Gilfedder et al., 2007a; Yoshida et al., 2007), soil (Yoshida et al., 2007), animal and macroalgae tissues (Hughes et al., 2006; Kaňa et al., 2015; Shah et al., 2005), edible salts (Yun et al., 2017; Zhang et al., 2010), and milk (Wang and Jiang, 2008). Previous measurements in ambient aerosols showed only three iodine species: I^-, iodate (IO_3^-) and total soluble organic iodine (SOI) and their relative concentration and size distribution varied largely with locations (e.g. inland, coastal or open ocean) (Baker et al., 2001; Gilfedder et al., 2007a, b; Lai et al., 2008; Wimschneider and Heumann, 1995; Xu et al., 2010). The majority of atmospheric models assume that IO_3^- would be the only stable and predominant iodine species in aerosols (Saiz-Lopez et al., 2012), because I^- may be eventually oxidized to IO_3^- in aerosols or participate in halogen activation to yield gaseous IX (X=Cl, Br, I). SOI deems to be formed from the reaction of aerosol organic matter with HOI (Baker, 2005b). Organic iodine compounds are more toxic than I^- and IO_3^- to humans (Ding and Zhang, 2009) and may play a key role in regulating the recycling of halogens to the gas phase. At present the speciation of organic iodine compounds is the most significant knowledge gap in aerosol iodine chemistry (Saiz-Lopez et al., 2012). Hence, to study the iodine speciation and size distribution will surely help to understand their sources, transformation mechanisms and deposition rates in the atmosphere.

It still poses a challenge to determine organic iodine compounds in ambient aerosol. Up to date, there is no detailed aerosol organic iodine speciation study in the literature. Total SOI was generally calculated as total soluble iodine minus inorganic I^- and IO_3^- (Lai et al., 2008), which can be separated and quantified using an ion chromatography coupled with inductively coupled plasma mass spectrometry (IC-ICP-MS). Although the peaks in

IC other than I^- and IO_3^- were suspected to be organic iodine (Gilfedder et al., 2007a, b, 2008), ICP-MS did not provide molecular weight information. Without foreknown information of ion mass, molecular structure or retention time (RT), neither liquid chromatography-MS (LC-MS) nor gas chromatography MS (GC- MS) can be applied to identify and quantify unknown organic iodine in the aerosols. Unlike those in disinfection by-products or iodine-rich seaweed, an individual organic iodine compound in a complex aerosol matrix is of extremely low concentration. Based on our experience, organic iodine ions co-elute with many other interfering ions even after chromatographic separation. As a result, it is difficult to apply even high resolution mass spectrometry to identify unknown organic iodine compounds in the aerosols using MS and MS/MS techniques.

The populated coastal regions of eastern China are influenced by both industrial and marine emissions. Growing algae population due to serious eutrophication in the coastal waters may promote iodine emission, which make the coastal region a potential hotspot of new particle formation. Up to now, there has been no report of iodine induced NPF in the places other than coastal sites of western Europe (e.g., Mace Head, Ireland; Roscoff, France; O Grove, Spain), Tasmania (Cape Grim) and Polar regions. Besides, the iodine speciation measurement in particles smaller than 100 nm is also scarce (Baker, 2005a; Baker, 2004; Gilfedder et al., 2008; Lai et al., 2008; Wimschneider and Heumann, 1995). The purpose of our study is to characterize iodine speciation using the ultra-performance liquid chromatography coupled with quadrupole time-of-flight mass spectrometry (UPLC/Q-TOF-MS) and measure their concentrations in size segregated particles down to 10 nm diameter collected during the NPF events observed at a coastal site of China. The comparison of iodine species between the coastal site and an inland site will also be discussed.

2. Experiments

2.1 Sampling

A five-month campaign from January to May 2018 was carried out at Xiangshan Gulf of Zhejiang Province on the east coast of China. The coastal observation site (29 °29’N, 121 °46'E, see Figure 1) is a small building about 40 m and 200 m away from the coastline at high tide and low tide, respectively. The Xiangshan Gulf is developed as the largest algae cultivation area of Zhejiang Province. This feature makes the Xiangshan Gulf a potential hotspot of iodine emission from wild or farmed algae. We used a scanning mobility particle spectrometer (SMPS) and a Neutral Air Ion Spectrometer (NAIS) to monitor NPF events at the site. The statistical characteristics of new particle formation at the observation site are not the focus of this paper. Instead, a nano Micro-Orifice Uniform Deposit Impactor (nano-MOUDI, MSP Corp, Shoreview, MN) or a median-volume aerosol sampler were used to collect size segregated 10 nm -18 μm aerosols or $PM_{2.5}$ during typical NPF days. The 13-stage nano-MOUDI provides d_{50} cut-off sizes of 18, 10, 5.6, 3.2, 1.8, 1.0, 0.56, 0.32, 0.18, 0.10, 0.056, 0.032, 0.018 and 0.010 μm in aerodynamic diameters when operating at a flow rate of 30 L min^{-1}. Offline method by high resolution mass spectrometer was developed to analyze iodine in the aerosol samples.

Particle size distribution from 2 nm to 740 nm was obtained by integrating a long SMPS (TSI DMA3081 and CPC3775; scanning range: 40-750 nm) and NAIS (scanning range:2-42nm) data. The SMPS sampled ambient air from a 129 cm long and 1.0 cm inner diameter (I.D.) SS tube horizontally oriented with an airflow of 14 standard L min^{-1}. NAIS sampling inlet was a 150 cm long and 32 cm inner diameter copper tube. The transport loss of particles in the SMPS and NAIS inlets was corrected using size-dependent survival ratios. Scanning cycles of the SMPS and NAIS were synchronized to 4 minutes. The NAIS measured positive ion, negative ion and total particles alternately. The classification of iodine-induced NPF (hereafter, I-NPF event) and continental NPF events was based on the size distribution observation and described in Section 3.1.

A nano-MOUDI sampling scheme was implemented according to the NPF classification. That is, one set of nano-MOUDI samples was collected during the continental NPF days from February 11 to 13; one set of nano-MOUDI samples was collected during the non-NPF days from April 16 to 18; one set of nano-MOUDI samples was collected during the I-NPF days from May 9 to 11 and three sets of daily $PM_{2.5}$ samples were collected during the I-NPF days from April 25 to 27. Each set of nano-MOUDI samples was collected continuously for 72 hours, during which I-NPF or continental NPF occurred on a daily basis, so aerosol chemical composition features of these two types of NPF events can be observed from offline analysis. In addition, as a comparison to the coastal site, four sets of $PM_{2.5}$ samples were randomly collected on January 14, April 15, April 25 and May 5 at an inland urban site 200 km from the coast (see Figure 1). The description of the inland site can be found in Yu et al. (2016). No simultaneous measurement of particle size distribution was made at the inland site.

The detailed sampling procedures for $PM_{2.5}$ and nano-MOUDI are as follows. $PM_{2.5}$ aerosols were collected on 90 mm quartz fiber filters using a median-volume aerosol sampler (TH-150C, Wuhan Tianhong Ltd., China) at a flow rate of 100 L min^{-1} for 23 h. Since quartz fiber filters may absorb volatile iodine species like hydrogen iodide (HI), which brings positive artifact to I^- measurement in aerosols, field blank filters were collected by placing a HEPA filter in the upper stream of a quartz fiber filter. Two nano-MOUDIs were placed side by side to collect 10-100 nm (stages 10-13) and 100 nm-18 μm (stages 1-9) aerosols, respectively. Considering low aerosol mass loading on stages 10-13, the chemical analysis of aerosols collected on 10-13 stages may be sensitive to the particle bounce-off from upper stages 1-9, Therefore, aluminum foil filters on the stages 1-9 of the first nano-MOUDI were silicon-greased to reduce potential bounce-off artifact on the filters of stages 10-13 that were sent for chemical analysis. For the second nano-MOUDI, all filters were not silicon-greased but only the filters of stages 1-9 were sent for chemical analysis. One set of field blank nano-MOUDI samples were also collected by drawing the air through the nano-MOUDI with a HEPA filter attached to the inlet. Before sampling, the filters were baked in a laboratory oven at ca. 500℃ for 24 h to remove organics. After sampling, the filters were packed and stored in a refrigerator below- 20℃.

2.2 Chemical analysis

A quarter or half of a filter was put in a 10 mL amber vial with 1:1 v/v mixture of water (LCMS grade, Aladdin, China) and methanol (LCMS grade, Adamas, China). The filter fraction was sonicated for 40 min and the extract was filtered by a 0.2 μm PTFE membrane syringe filter. The eluate was evaporated to almost dryness in a rotary evaporator below 40℃ and subsequently re-dissolved in 0.5 mL water. After being centrifuged (12000 rpm) for 30 min, the supernatant was collected for MS analysis using a Waters UPLC (BEH column, 1.7μm column, 2.1×50mm) coupled with a Xevo G2 Q-TOF MS. A gradient eluent at flow rate 4mL/min was applied as below: 2/98 methanol/water for 0.5 min, linearly increased to 98/2 over 9.5 min, 98/2 held for 2 min, and returned to 2/98 for 3 min. The MS was operated in either positive or negative mode with a TOF resolving power of 32000 FWHM (ESI+) or 28000 FWHM (ESI-). The MS was externally calibrated daily in the mass range 50–1200 using a 0.5 mM sodium formate solution. A real time Lockmass correction was applied by acquiring leucine-enkephalin spectrum from a lock spray source. Optimized source parameters were as follows: capillary voltage −2.5 kV for ESI- (or +3.0 kV for ESI+), desolvation gas flow 600 L h^{-1} with temperature 450 ^{o}C and source temperature 120 °C. Depending on the purpose, the QTOF was operated in 3 modes: low energy MS scan mode (in which molecular ions are subject to in-source fragmentation only), high energy MS scan mode (in which molecular ions are subject to both in-source fragmentation and collision induced dissociation) and MSMS mode (in which selected precursor ions are subject to fragmentation with collision induced dissociation before entering TOF). Collision cell voltage was scanned from 10 to 40 eV. Mass spectrum was acquired as continuum format and analyzed by the MassLynx

4.1 software. The procedure of identification and semi-quantification of iodine species will be explained in detail in Section 3. To validate the semi-quantification by our procedure, 20 samples with relatively high iodine concentration were also analyzed for total soluble iodine using Agilent 7500a ICP-MS (Agilent Technologies, Santa Clara, CA, USA). To do that, 200 µl aerosol extract was diluted to 5 ml for injection and the iodine detection limit of the ICP-MS was 0.1 µg L^{-1}.

3. Result and discussion

Section 3.1 first discusses particle number size distribution patterns of two types of NPF events at the coastal site. Section 3.2 discusses the identification and semi-quantification of iodine species in the ambient aerosols. The speciation and size distribution of iodine species during the two types of NPF events at the coastal site are shown in Section 3.3. The comparison of iodine species between the coastal site and the inland site is discussed in Section 3.4.

3.1 Particle number size distribution patterns of iodine-induced NPF and continental NPF events

Based on the particle size distribution data, we identified two types of NPF events. The first type of NPF events was observed on 7 out of 54 non-raining observation days during the cold season from January to March. Figure 2a shows the typical particle number size distributions of this type of NPF events from February 11 to 13. As we can see in Figure 2a, the production of 2-7 nm neutral particles began at 8:00~9:00 and ceased at around 15:00. New particle formation appeared to be not associated with the low tide, but followed a nearly identical variation with both solar radiation and daytime tide height. After the formation, new particles grew to about 100~200 nm in the middle of the night, following a typical banana-shape contour (Figure 2a, 1st row). These features, together with the air mass backward trajectories originating from northwest inland of China (Figure S2), confirm that this was a regional-scale continental NPF event. Air mass backward trajectories were computed using the HYSPLIT (Hybrid Single-Particle Lagrangian Trajectory, NOAA/ARL) model (Draxler and Rolph 2003). $N_{2\text{-}20}$, number concentration of 2-20 nm particles, reached up to 7×10^4-1.3×10^5 cm^{-3} during this type of NPF events, which is higher than the average $N_{3\text{-}20}$ 2.5×10^4 cm^{-3} during the continental NPF events recorded by us at Nanjing, the inland urban site in 2016 (Dai et al., 2017).

Strong NPF events were observed on 24 out of 33 non-raining observation days in April and May, which is the growth and farming season of seaweed. That is, the second type of NPF events occurred almost every day from April to May unless it was cloudy or rainy. As would be discussed in Section 3.3, high nucleation-mode iodine concentration suggests these NPF events were induced by iodine. Figure 2b shows the typical particle number size distributions from May 8 to 10. As can be seen, the production of 2-7 nm began at 9:00~10:00 and lasted until 18:00. There is a clear time lag of ~4 hours between solar radiation increase and the production of 2-7 nm. High $N_{2\text{-}7}$ (number concentration of 2-7 nm particles) seemed to be associated with low tide during 13:00-15:00. $N_{2\text{-}20}$ reached up to 7×10^6 cm^{-3}-1×10^7 cm^{-3}, which is two orders of magnitude higher than those during the continental NPF. The peak $N_{2\text{-}20}$ values at this coastal site are also one order of magnitude higher than those recorded during the most intense I-NPF events at Mace Head, Ireland (5×10^5-1×10^6 cm^{-3}) (O'Dowd et al., 2002). A clear nucleation mode below 30 nm was seen on each sampling day and particles rarely grew beyond 30 nm at the coastal site of our study. The "interrupted" growth pattern suggested that the NPF was limited in a relatively small area around the site. Wild and farmed algae at the Xiangshan Gulf were likely the source of these high concentration nucleation mode particles. In particular, during the harvesting season, the wet algae have to be dehydrated by exposing them to sunlight for a few days before further processing or transportation. During this process, a large amount of iodine vapors can be emitted and oxidized to produce new particles.

It has been reported from both field and laboratory studies that I-NPF is initiated by a pure negative ion nucleation of HIO_3 (Sipilä et al., 2016). We examined neutral, positive and negative nanoparticle concentrations measured by NAIS during the two types of events. It has been found that during the I-NPF events the negative ion concentrations were 100±102%, 8±13% and 58±32% higher than those of positive ions in the size ranges of 0.8-2 nm, 2-7 nm and 7-20 nm, respectively. On the other hand, negative and positive ion concentrations in all above-mentioned size ranges were almost the same during the continental NPF events (Figure 2a, row 4-6). The neutral particle concentrations during I-NPF events were higher than those in continental NPF events by two orders of magnitude; however, the ion concentrations were similar in both types of NPF events, which were in the concentration range of 100-1000 cm^{-3} in all size bins. As a result, the ion/neutral particle ratios were on the order of 10^{-5} (2-7 nm) and 10^{-4} (7-20 nm) during the I-NPF events and 10^{-3} (2-7 nm) and 10^{-2} (7-20 nm) during the continental NPF events, indicating the contribution of ions to total particles was negligible at least in > 2 nm size range in both types of NPF events.

3.2 Iodine speciation and semi-quantification

The high resolution LC-MS offers the prospect of identifying unknown organic compounds in complex samples. Previous studies identified unknown organic iodine compounds in disinfected drinking water and seaweed base on a strategy that the retention time and accurate mass of iodine-containing precursor ions can be selectively determined by searching their product ion I^- (m/z 126.9) in MS/MS experiments (Ding et al., 2009; Yang et al., 2016). Unfortunately, their strategy does not work for our aerosol samples because of two difficulties. First, we found that most of iodine-containing ions in our samples were dissociated to release I^- due to in-source fragmentation even in the most gentle ionization condition (e.g., low capillary voltage, low source temperature and desolvation temperature). This can been seen from Figure 3a that extracted ion chromatograms of m/z 126.9039 are of similar intensity in low energy MS scan mode (in-source fragmentation only) and high energy MS scan mode (in-source fragmentation plus collision induced dissociation). In this situation, it is impossible to select unfragmented iodine-containing precursor ions for MSMS experiments. Second, even if organic iodine compounds can survive from in-source fragmentation, there are many co-eluting background interfering ions. It is time and labor consuming to search I^- from all co-eluting molecular ions using MSMS experiments. This often becomes impractical because small organic iodine ions and other neighboring ions often appear in the same precursor isolation window of quadrupole.

Iodide-organic adducts

For reversed phase HPLC, ionic compounds elute earliest followed by non-ionic organics with longer retention time. In our case, ionic I^-, IO_x^- and other strong Lewis acids elute with RT<1 min, as can be seen from the extracted m/z 126.9039 chromatogram of pure potassium iodide solution (1 mmol L^{-1}) in Figure 3b. The I^- peaks that eluted at RT>1 min in low energy MS scan mode (Figure 3a), on the other hand, can only be resulted from the dissociation of weakly bound iodine-containing organic precursors via in-source fragmentation. I^- is an electronegative weak base, which can bind with hydroxyl, acid or keto- groups to form adducts depending upon the polarity and H-bonding capability of organic compounds (Lee et al., 2014). These iodine-containing organics that dissociated to release I^- in the ESI source are thus attributed to iodide-organic adducts in our study and the total peak area of extracted ion chromatogram of m/z 126.9039 after RT 1 min is assumed to be proportional to their total concentration. Our experiment presented in Figure 3b-3d partly supported the above hypothesis. No I^- peak was detected after RT 1 min in the extracted m/z 126.9039 chromatograms of pure KI solution (1 mmol L^{-1}, Figure 3b) or an aerosol extract with low concentration of iodine (Figure 3c). However, when the aerosol extract was mixed with KI solution for another analysis, elevated I^- peaks in low energy MS scan mode (blue line, Figure 3d) indicated the formation of iodide-organic adducts. Furthermore, when collision induced dissociation was applied, no additional I^- peaks showed up in high energy MS scan mode (red line, Figure 3d). Such an observation implies that (1) iodide-organic adducts were formed in the aerosol extract+KI mixture but were easily dissociated in the low energy MS scan mode and (2) no stable organic iodine compounds were formed in the aerosol extract+KI mixture. This is also confirmed by the fact that no new ions were formed by comparing the mass spectra of aerosol extract before and after KI addition.

Organic iodine compounds

On the other hand, the identities of those stable organic iodine compounds, i.e., the compounds with C-I bond that are not or partially dissociated in the ESI source, are still unknown but their atmospheric chemistry may be of more interest. To bypass the difficulty as discussed above, a signal amplification approach has been applied in this study to identify these unknown organic iodine compounds, for which the detailed steps are shown in Figure 4. The approach is analogous to searching a secondary organic aerosol (SOA) tracer in ambient aerosols after its identity as VOC oxidation product is confirmed by smog chamber simulation. A portion of low iodine aerosol extract+KI mixture was added with H_2O_2 solution (10 mmol L^{-1}). After reaction for 4 h, the mixture was injected for low and high energy MS scans. As compared to the chromatograms of the untreated mixture (Figure 3d), a considerable amount of stable organic iodine compounds were formed but dissociated only in high energy MS scan (red curve in Figure 3e), in addition to the formation of more iodide-organic adducts (low energy MS scan, blue curve in Figure 3e). These organic iodine compounds are believed to be from the reactions between aerosol organics and HOI that is produced via H_2O_2+I^- reaction.

The identities of these organic iodine compounds can be obtained by comparing MS scan mass spectra (low energy) before and after the H_2O_2 addition using mass defect (MD) *vs.* m/z diagram. The mass spectrum was reconstructed by integrating over RT 0-15 min. All ions above background intensity of 10^4 are shown in Figure 5 as dots and circles to stand for the samples before and after H_2O_2 addition, respectively. Benefiting from the large negative mass defect of iodine (-0.0961), the mass defects of newly-formed organic iodine compound should be in the range of -0.3~0, which makes them to be distinguished easily from non-iodine containing ions. Therefore, each red circle without a black dot in -0.3~0 mass defect range in Figure 5 should stand for an organic iodine compound that was newly formed after the addition of H_2O_2 into aerosol extract+KI mixture. These potential organic iodine ions were further selected for MSMS experiments to confirm that their fragments contained I^-. Since mass assignment is more accurate for an amplified symmetrical peak than a small shoulder peak, the amplification of organic iodine compound concentrations helps to obtain accurate masses of potential iodine organic compounds in ambient aerosols. After that, their retention time information in the UPLC was acquired by extracting their ion chromatograms from low energy MS scan data. Following the same procedure, two $PM_{2.5}$ samples collected at the inland site and two $PM_{2.5}$ samples collected at the coastal site were treated using KI and H_2O_2 (or O_3 solution) and analyzed using MD *vs.* m/z diagrams in both ESI+ and ESI- modes (Step 1, Figure 4).

In step 2, the elemental compositions of organic iodine compounds were calculated from the accurate masses within 1 mDa mass tolerance allowing the elements C, H, N, O, S and I and confirmed by their isotope patterns. The correctness of calculated molecular formulas was further restricted by the matching of at least one sound structure in ChemSpider database. Consequently, a total of 80 formulas (57 in negative mode and 23 in positive mode) were obtained, each of which should represent an organic iodine compound and its isomers. Because both H_2O_2 and O_3 are important oxidants in atmospheric aerosols, the organic iodine compounds formed in Step 1 may also exist in real aerosol samples via the same reaction mechanism in the atmosphere. Therefore, in Step 3 these newly identified 80 formulas were searched in real aerosol samples using a targeted screening strategy based on their accurate mass and retention time. At last, 35 organic iodine formulas were detected, at least once, in our aerosol samples including the $PM_{2.5}$ samples and the size-segregated aerosol samples from all nano-MOUDI stages

(Table 1). The other formulas were not detected in any of the aerosol samples, probably due to their slower production rate or the absence of corresponding organic precursors in the atmosphere. The number of isomers listed in the second column of Table 1 is based on the number of ion chromatographic peaks observed for given m/z values in the real aerosol samples. The total 45 isomer peaks, as well as their retention times, are shown in Figure S1. Hence, there are in total 45 organic iodine compounds detected in our samples.

As shown in Table 1, 35 molecular formulas were classified into four groups: 5 non-aromatic formulas and 30 aromatic formulas including 16 CHOI formulas, 3 CHNI formulas and 11 CHONI formulas. The 5 non-aromatic formulas are assigned to iodoacetic acid, diiodoacetic acid, iodopropenoic acid, iodomethanesulfonic acid and diiodomethane. The first 4 compounds are electrophilic substitution products of alpha-H of organic acids by I^+ from HOI or I_2. Diiodomethane is probably from gas-particle partitioning or the product of iodoform reaction of methyl ketones. Iodoacetic acid was identified in 9 of 10 samples collected from the coastal and inland sites. The other 4 non-aromatic compounds, however, were mostly found at the coastal site.

30 CHOI, CHONI and CHNI formulas are assigned to aromatic compounds that are prone to electrophilic substitution by I^+. The formulas observed in ESI- mode are expected to have a carboxyl or phenol group, while those observed in ESI+ mode should be aromatic or heterocyclic amines. 16 CHOI formulas are iodinated phenols, substituted benzoic acids or phenolic acids. The 3 most frequently detected formulas are $C_8H_7O_2I$, $C_7H_5O_4I$, $C_7H_5O_2I$. CHONI formulas with 3-5 O atoms detected in ESI- mode are iodinated nitrophenol, nitronaphthol or nitrobenzoic acid. CHONI formulas with 1 O atom detected in ESI+ mode are iodinated hydroxyaniline, pyridinol, or quinolinol. The most frequently detected CHONI compounds are $C_6H_4NO_4I$, $C_{10}H_6NO_3I$ and $C_6H_4NO_3I$. CHNI formulas are heterocyclic amines (i.e., pyrazoles, imidazoles and triazoles), among which $C_7H_{11}N_2I$ was detected in 4 out of 10 samples.

Further assignment of the exact identity for the above formulas is impractical, because these 35 molecular formulas probably stand for hundreds of isomers, for most of which no commercial standards are available. Nevertheless, the identities of 4 compounds have been confirmed including iodoacetic acid ($C_2H_3O_2I$), 3-iodo-2-propenoic acid ($C_3H_3O_2I$), 3-iodo-benzoic acid ($C_7H_5O_2I$) and 2-hydroxy-5-iodopyridine (C_5H_4NOI) according to the retention times of their commercial standards. These 4 compounds are identifiable because they have no or very few isomers, of which the commercial standards can be procured. Subsequently, these four compounds can be used as surrogate standards to semi-quantify the concentrations of other organic iodine species.

Inorganic iodine species

In addition to the above organic iodine compounds, some inorganic iodine species were also detected. Figure 6 shows the integrated mass spectrum of molecular ions between RT 0.5-0.7 min obtained by low energy MS scan of an S13 nano-MOUDI sample (10-18 nm particles) collected during the I-NPF days. The most abundant species is IO_3^-, followed by I^- and HSO_4^-. I_3^- was also observed, probably due to the adduct formation between I^- and I_2. IO_2^- and IO^- are detectable, but their abundances are two orders of magnitude lower than IO_3^-. Iodine oxides $I_2O_{2\text{-}5}$ were not ionizable by the ESI source, but they might have been hydrated to HIO_x and detected as IO_x^- (Sipilä et al. 2016). Iodide-metal complexes like CuI_2^-, $Cu_2I_3^-$, ZnI_3^- and $CuI_2(HCN)(HCl)^-$ were observed in $PM_{2.5}$ samples but not in size-segregated nano-MOUDI samples. Cu^+ and Zn^{2+} are typical coarse mode components. The observation thus indicated that the iodide-metal complexes detected in the $PM_{2.5}$ samples were formed only after fine- and coarse-mode components were mixed in the sample extract. To avoid artificial formation of iodide-metal complexes during the sample extraction process, our result highlights the importance of collecting $PM_{0.5}$, PM_1 or size-segregated samples instead of $PM_{2.5}$ or PM_{10}.

Semi-quantification of identified iodine species

So far 35 organic iodine formulas (45 isomer peaks) and 5 inorganic iodine anions have been identified. In order to know their size distributions and relative abundances in different types of samples, the following strategy was applied to semi-quantify these iodine species (step 4, Figure 4): external calibration curves of peak area *vs.* concentration were established by analyzing standard solutions of KI, KIO_3, iodoacetic acid, 3-iodo-2-propenoic acid, 3-iodo-benzoic acid and 2-hydroxy-5-iodopyridine. I^-, I_3^- and iodide-organic adducts were quantified using KI as a surrogate standard by assuming their ionization efficiencies are similar in ESI- mode. The peak area of iodide-organic adducts was calculated as the total peak area of extracted ion chromatogram of m/z 126.9039 after RT 1 min. Iodide-metal complexes like CuI_2^-, $Cu_2I_3^-$, ZnI_3^- and $CuI_2(HCN)(HCl)^-$, if present, were also quantified using KI but counted as I^-. IO_3^-, IO_2^- and IO^- were quantified using KIO_3 by assuming iodate, iodite and hypoiodite have similar ionization efficiencies. Iodoacetic acid and 3-iodo-2-propenoic acid were quantified with their respective standards. The other 3 non-aromatic compounds diiodoacetic acid, iodo-methanesulfonic acid and diiodomethane were quantified using surrogate standard iodoacetic acid. All CHO and CHNO compounds observed in ESI- mode were quantified using 3-iodo-benzoic acid, because they have similar structure of a carboxyl or phenol group attached to aromatic rings. All CHNO and CHN compounds observed in ESI+ mode were quantified with 2-hydroxy-5-iodopyridine by assuming these aromatic or heterocyclic amines have similar ionization efficiencies. Due to the low amounts of individual aromatic compounds, a total concentration of all aromatic iodine compounds detected was presented for each sample. Field blank filters were processed in the same way as sample filters. No signals above MS background were detected in the field blank filters for the iodine species other than I^- and IO_3^-. The MS signals of I^- and IO_3^- in the field blanks were comparable to those in the sample filters without iodine loading (e.g., the nano-MOUDI filters in the size bins larger than nucleation mode during the I-NPF days), but less than 1.3% of those in the sample filters with iodine loading. The MS signals of I^- and IO_3^- in the field blank were then subtracted from the aerosol samples.

There are a few limitations in the above-mentioned strategy. First, the use of surrogate standards can only be regarded as semi-quantification for unassigned species. Second, it is still possible that some unknown organic iodine compounds are missed by our method shown in Figure 4. Third, inorganic iodine ions that elute around 0.5-0.7 min are prone to a stronger matrix ion suppression effect than organic compounds. The underestimation may be the most serious if there are high concentrations of co-eluting sulfate, nitrate and ammonium in the aerosol samples of accumulation mode. After UPLC/Q-TOF-MS measurement, we selected 13 samples with relatively high iodine concentrations for ICP-MS analysis, including 3 $PM_{2.5}$ samples and 10 size-segregated samples from 10 nm to 1.8 μm collected during the NPF days. A linear regression analysis was conducted between the sum of all iodine species measured by this method and the total iodine measured by ICP-MS. As shown in Figure 7, the total iodine concentration analyzed by our method is 90.5% on average of that obtained by ICP-MS with a R^2 of 0.94. In spite of the above uncertainties, our method provided a lower-limit estimate of iodine concentrations in ambient aerosols.

3.3 Concentration and size distribution of iodine species during the NPF days at the coastal site

We compared the total concentrations (Figure 8) and mass size distributions (Figure 9) of iodine species in 10 nm-18 μm particles during the I-NPF, continental NPF and non-NPF days at the coastal site. The particle number size distributions during the same NPF days have been shown in Figure 2. It should be noted that, identical to previous aerosol iodine speciation studies, the concentration reported here (pmol m^{-3}) is an average over the entire period of 3 sampling days. Thus, iodine concentrations during the intense NPF periods should be higher than the values reported in this work. Continuous mass size distribution was fitted from the measured size-segregated mass concentration data by assuming multimodal lognormal size distributions (Yu et al. 2010). Size distribution of sulfate (HSO_4^-) was also shown (μg m^{-3}) in Figure 9. Although not highly accurate, relative distribution in different sizes is less affected by the uncertainties of semi-quantification.

The highest total iodine concentration 126.3 pmol m^{-3} was found during the I-NPF days, which was 3.1 and

5.5 times higher than those during the continental NPF and non-NPF events, respectively. As shown in Figure 9a, all iodine species except iodoacetic acid were characterized by a nucleation mode with mode diameters between 22-35 nm during the I-NPF days. This clearly shows that iodine was the NPF precursor in this type of NPF events. The most remarkable iodine species during the I-NPF days is IO_3^- with a mole fraction of 42.5%. This is consistent with the recent observation that HIO_3 is the key nucleating precursor in I-NPF event (Sipilä et al., 2016). On the other hand, the sum of iodide ($[I^-]+[I_3^-]$) and iodide-organic adducts accounted for ~50 % of total iodine in newly formed iodine particles. The presence of high iodide concentration in clusters or new particles has not been reported by previous field or laboratory measurements using CI-Api-TOF or AMS (O'Dowd et al., 2002; Mcfiggans et al., 2004; Sipilä et al., 2016). Iodide is most likely originating from the partitioning of gaseous precursor HI formed during the photolysis of I_2 or iodomethane. HI itself is not a good nucleation precursor due to the lack of H-bond or halogen bond, but our measurement suggests that HI might contribute to new particle growth in the size range as small as 10-18 nm. The finding of HSO_4^- in nucleation mode (Figure 6 and 9a) indicates that H_2SO_4 also contributed to new particle growth during the I-NPF days. This is consistent with previous laboratory observations of efficient uptake of H_2SO_4 onto humidified iodine oxide particles below 20 nm (Saunders et al. 2010).

Although organic iodine compounds were most frequently found in the I-NPF samples (Table 1), they accounted for only 6.8% of total iodine in the newly formed iodine particles. Considering the short lifetime of new particles in the atmosphere, organic iodine compounds were most likely from the heterogeneous uptake of gaseous HOI (formation route: I →IO →HOI) and subsequent reactions with organics in the new particles. One exception is iodoacetic acid that was characterized by a smaller accumulation mode and a larger coarse mode. Backward trajectory analysis showed that air masses moved from the open ocean of East China Sea during the I-NPF days (Figure S2). The unique size distribution of iodoacetic acid indicates that direct sea salt emission was probably its major source.

Lower iodine concentrations during the continental NPF days and non-NPF days might be due to relatively low iodine emission rate or transformation rate (from gaseous emission to particles) in non-algae-growth season or cloudy days. Iodine during the continental NPF days was characterized by an accumulation mode with mode diameters between 500-700 nm (Figure 9b), except that iodoacetic acid had a coarse mode and 3-iodo-2-propenoic acid had a 60 nm Aitken mode. The absence of nucleation mode for most of iodine compounds implies that iodine was unlikely to be an important NPF precursor in the continental NPF. Despite different size distribution from I-NPF, the mole fraction of iodide and iodide-organic adducts were again ~50% of total iodine during the continental NPF. The outstanding species in the continental NPF days were aromatic iodine compounds that accounted for 30% of total iodine. This is not surprising because air masses from inland areas of China on these days might contain a large amount of anthropogenic aromatic substances. Upon arrival in the coastal region, the uptake of gaseous HI, HOI or $IONO_2$ onto these anthropogenic particles and the subsequent aerosol phase reactions between I^-, H_2O_2/O_3, HOI and aromatic compounds are hypothesized to be the formation mechanism of aromatic iodine compounds.

Iodoacetic acid and 3-iodo-2-propenoic acid surprisingly accounted for 44.3% of total iodine concentration (22.8 pmol m^{-3}) during the non-NPF days. The high iodoacetic acid concentration, together with its presence in coarse mode, again suggests its unique source associated with sea salt emission. 3-iodo-2-propenoic acid during the non-NPF days and continental NPF days was characterized by a bimodal distribution with mode diameters around 1 μm and 50-63 nm. In contrast, the bimodal distribution was replaced by a single small nucleation mode during the I-NPF days. The sources of 3-iodo-2-propenoic acid and iodoacetic acid became more important during the non-NPF days and merit more investigation.

3.4 Comparison between coastal site and inland site

Table 2 gives a comparative overview of iodine species in $PM_{2.5}$ between the inland urban site and the coastal site. The coastal samples include the 3 sets of nano-MOUDI data presented in Figure 8, from which the concentrations of various iodine species in 10 nm - 3.2 μm particles were extracted to approximate $PM_{2.5}$; the rest of data were acquired by directly analyzing the $PM_{2.5}$ samples. It is found that total iodine was in the range of 6.5-11.2 and 19.5-122.6 pmol m^{-3} at the inland and coastal sites, respectively. Larger variation of iodine concentrations at the coastal site is due to the inclusion of both I-NPF and non-NPF samples. The concentrations of nearly all iodine species at the inland site were lower than those at the coastal site. This indicates that there were no or relatively weak iodine emission sources surrounding the inland site. Our total iodine concentrations are in the same order of magnitude as those reported at Mace Head (10-532 pmol m^{-3}, Gilfedder et al., 2008), an Ireland coastal site where iodine NPF has long been reported, and Regensburg, an inland site of southern Germany (15.7-61.3 pmol m^{-3}, Wimschneider and Heumann, 1995), although their maximum values are higher than ours.

A negligible amount of iodate (1.1%) was detected in only 1 out of the 4 inland samples. In fact, the concentration of iodate was also low on the days without I-NPF events at the coastal site (on average 7 ± 1%). Therefore, iodate is a predominant species only in newly formed particles (Figure 9) and its concentration might be reduced soon in the aging process via reactions like $IO_3^- + I^- + 6H^+ \rightarrow 3I_2 + 3H_2O$ (Pechtl et al., 2007). The mole fractions of iodide were 23 ± 9% and 31 ±14% at the inland and coastal sites, respectively. Following the old definition, the iodine species other than I- and IO_3^- were calculated as soluble organic iodine (SOI). Our finding is that newly formed iodine particles were mostly composed of inorganic I^- and IO_3^- (68 ±20 % of the total iodine), but SOI fraction increased to account for on average 76 ±7% of total iodine in the aged particles. Among the SOI species, the largest fraction 64 ± 8% was attributed to iodide-organic adducts at the inland site, followed by aromatic iodine (12 ± 3%) and iodoacetic acid (1.6 ±1.0%). All other species were not detectable or of negligible amounts.

Table 2 clearly shows that more information on the speciation of soluble organic iodine in the aerosol samples is provided in this study as compared to previous studies. In particular, a portion of iodine technically defined as iodide-organic adducts was reported in our study for the first time, because they cannot survive in electrospray ionization processes even in the most gentle source conditions, due to the weak bounding strength of I^- with organics. I-organic adducts accounted for 64 ± 8% in the inland urban samples and 31 ± 16% in the coastal samples. Using IC-ICP-MS method, this portion of iodine is likely counted towards organic iodine compounds. Our analysis shows that this portion of iodine adducts can be attributed to neither stable organic iodine compounds nor free I^- ion. Under certain condition, e.g., pH value, iodide-organic adducts probably release free I^- ion in the ambient aerosols.

4. Conclusion

Intense new particle formation events were observed during the algae growth and farming season at Xianghshan Gulf, a coastal algaculture area of China. The high iodine concentration in nucleation mode particles measured by UPLC/Q-TOF-MS confirmed that the NPF events were induced by iodine species. This is the first study to investigate iodine-induced NPF in a place other than the coastal locations of western Europe, Tasmania and Polar regions. China produced 58% of global cultivated seaweed production (11 million tons in 2010, Nayar and Bott, 2014). Iodine is likely emitted to the atmosphere and transformed to nano particles during the farming, harvesting and processing of cultivated seaweed. Growing algae population due to serious eutrophication in the coastal waters of China also promotes iodine emission. Therefore, wild algae, as well as farmed algae, could be an important source of new particle formation in the coastal areas of China.

Using UPLC/Q-TOF-MS, inorganic I^-, IO_x^- and I_3^- were easily identified according to their accurate ion mass. A large portion of iodide was observed to exist as weakly bound iodide-organic adducts. A signal amplification approach was applied to look for organic iodine compounds, i.e., the compounds with C-I bond. For the first time, 35 molecular formulas, or 45 organic compounds according to the number of isomer peaks, were identified in ambient aerosols. Iodine species on the I-NPF days and continental NPF days were characterized by a nucleation mode and an accumulation mode, respectively. For the first time, high concentration of I^- was observed in particles as small as 10-18 nm, suggesting gaseous HI may contribute to new particle growth in the I-NPF events. Iodate was a remarkable species in only newly formed particles and was reduced in the aging process. Newly formed iodine particles were mostly composed of inorganic I^- and IO_3^-, but SOI ([total iodine]-[I^-]-[IO_3^-]) accounted for the majority of iodine in the aged particles. Generally speaking, organic iodine compounds resided in the same particle mode as inorganic iodide. It is still not clear whether organic iodine compounds contributed to nucleation or just the growth of new particles via iodine reactions with organics. During the continental NPF days, the outstanding iodine species is aromatic iodine compounds in the accumulation mode that accounted for 30% of total iodine. Those aromatic iodine compounds were probably formed from aqueous phase reactions between I^-, H_2O_2/O_3, HOI and aromatic organic compounds during in-cloud processing. The unexpected iodoacetic acid in the coarse mode that direct sea salt emission was probably its major source.

Our study provided important information of iodine speciation, concentration and size distribution in the context of heavy air pollution in China’s coastal areas. However, source, gas-particle partitioning and the role of these iodine species in NPF are largely speculative. Moreover, the chemical composition and the role of iodine in cluster sizes (1-3 nm) are still unknown. Simultaneous measurement of gaseous iodine precursors like I_2, HI, HIO_x and IO_x using online instruments like CI-Api-TOF and DOAS are needed to elucidate the above questions. On the other hand, more field measurements at multiple sites are required to test on what spatial scale iodine NPF might be of relevance, in competition with other NPF precursors.

Author contribution

H.Y. and H.X. designed and organized the study. X.H. and L.R. conducted the field measurements. H.Y. and L.R. performed the instrument experiments and data analysis. H.Y. and L.R. wrote the paper. M.X. and J.H. contributed to data interpretation and paper writing.

Acknowledgements

The authors would like to thank the National Key Research and Development Program of China (2016YFC0203100) and the National Science Foundation of China (grant numbers. 41675124).

References

Allan, J.D., Williams, P.I., Najera, J., Whitehead, J.D., Flynn, M.J., Taylor, J.W., Liu, D., Darbyshire, E., Carpenter, L.J., Chance, R., Andrews, S.J., Hackenberg, S.C., McFiggans, G.: Iodine observed in new particle formation events in the Arctic atmosphere during ACCACIA, Atmos. Chem. Phys., 15, 5599-5609, doi: 10.5194/acp-15-5599-2015, 2015.

Baker, A.: Marine aerosol iodine chemistry: The importance of soluble organic iodine, Environ. Chem., 2, 295-298, doi: 10.1071/EN05070, 2005.

Baker, A.R.: Inorganic iodine speciation in tropical Atlantic aerosol, Geophys. Res. Lett., 31, 187-206, doi:10.1029/2004GL020144, 2004.

Baker, A.R., Sj, C.M.P., Jickells, T.D., Thompson, D.: Iodine concentration and availability in atmospheric aerosol, Atmos. Environ., 34, 4331-4336, doi: 10.1016/s1352-2310(00)00208-9, 2000.

Baker, A.R., Tunnicliffe, C., Jickells, T.D.: Iodine speciation and deposition fluxes from the marine atmosphere, J. Geophys. Res-Atmos., 106, 28743-28749, doi: 10.1029/2000JD000004, 2001.

Burkholder, J., Curtius, J., Ravishankara, A., Lovejoy, E.: Laboratory studies of the homogeneous nucleation of iodine oxides, Atmos. Chem. Phys., 4, 19-34, doi: 1680-7324/acp/2004-4-19, 2004.

Chen, Z.L., Megharaj, M., Naidu, R.: Speciation of iodate and iodide in seawater by non-suppressed ion chromatography with inductively coupled plasma mass spectrometry, Talanta, 72, 1842-1846, doi:10.1016/j.talanta.2007.02.014, 2007.

Dai, L., Wang, H., Zhou, L., An, J., Tang, L., Lu, C., Yan, W., Liu, R., Kong, S., Chen, M.J.: Regional and local new particle formation events observed in the Yangtze River Delta region, China: Simultaneous NPF measurementsat 2 sites, J Geophys. Res-atmos., 122(4):2389-2402, doi: 10.1002 /2016JD026030, 2017.

Dall'Osto, M., Simo, R., Harrison, R. M., Beddows, D. C. S., Saiz-Lopez, A., Lange, R.,Skov, H., Nøjgaard, J. K., Nielsen, I. E., and Massling, A.: Abiotic and biotic sources influencing spring new particle formation in North East Greenland, Atmos. Environ., 190, 126-34, doi:10.1016/j.atmosenv.2018.07.019, 2018.

Draxler R R, Rolph G D: HYSPLIT-hybrid single particle lagrangian integrated trajectory model 2003 (NOAA Air Resources Laboratory: Silver Spring, MD) http://ready.arl.noaa.gov/HYSPLIT.php, 2003.

Ding, G., Zhang, X.: A picture of polar iodinated disinfection byproducts in drinking water by (UPLC/)ESI-tqMS,Environ. Sci. Technol., 43, 9287, doi:10.1021/es901821a, 2009.

Dixneuf, S., Ruth, A.A., Vaughan, S., Varma, R.M., Orphal, J.: The time dependence of molecular iodine emission from Laminaria digitata, Atmos. Chem. Phys., 9,823-829, doi:10.5194/ acp-9-823-200 9, 2009.

Gilfedder, B. S., Lai, S. C., Petri, M., Biester, H., Hoffmann, T.: Iodine speciation in rain, snow and aerosols, Atmos. Chem.Phys., 8, 6069-6084, doi: 10.5194/acp-8-6069-2008, 2008.

Gilfedder, B.S., Petri, M., Beister, H.: Iodine Speciation in Rain and Snow, Nucl. Atmos. Aero., doi: 10.1007/978-1-4020-6475-3_108, 2007a.

Gilfedder, B.S., Petri, M., Biester, H.: Iodine speciation in rain and snow: Implications for the atmospheric iodine sink, J. Geophys. Res-atmos.,112, doi:10.1029/2006JD007356, 2007b.

Grose, M.R., Cainey, J.M., McMinn, A., Gibson, J.A.E.: Coastal marine methyl iodide source and links to new particle formation at Cape Grim during February 2006. Environ Chem 4, 172-177.doi: 10.1071/EN07008, 2007

Hughes, C., Malin, G., Nightingale, P.D., Liss, P.S.: The Effect of Light Stress on the Release of Volatile Iodocarbons by Three Species of Marine Microalgae, Limnol. Oceanogr., 51, 2849-2854, doi:10.4319/lo.2006.51.6.2849, 2006.

Kaňa, A., Hrubá, L., Vosmanská, M., Mestek, O.: Analysis of iodine and its species in animal tissues, Chemical. Spec. Bioavailab., 27, 81-91, doi: 10.1080/09542299.2015.1087160, 2015.

Lai, S.C., Hoffmann, T., Xie, Z.Q.: Iodine speciation in marine aerosols along a 30,000 km round‐trip cruise path from Shanghai, China to Prydz Bay, Antarctica, Geophys. Res. Lett., 35, L21803, doi:10.1029/2008gl035492, 2008.

Lee, B. H., Lopez-Hilfiker, F. D., Mohr, C., Kurtén, T., Worsnop, D. R., and Thornton, J. A.: An Iodide-Adduct High-Resolution Time-of-Flight Chemical-Ionization Mass Spectrometer: Application to Atmospheric Inorganic and Organic Compounds, Environ. Sci. Technol., 48(11).48,6309-6317, doi:10.1021/es5003 62a, 2014.

Liu, W., Yang, H., Li, B., Xu, S.: Determination of Bromine and Iodine Speciation in Drinking Water Using High Performance Liquid Chromatography‐Inductively Coupled Plasma‐Mass Spectrometry, Geostand. Geoanal. Res, 35, 69-74., doi:10.1111/j.1751-908X.2010.00033.x, 2015.

Mahajan, A.S., Sorribas, M., Gómez Martín, J.C., MacDonald, S.M., Gil, M., Plane, J.M.C., Saiz-Lopez, A.: Concurrent observations of atomic iodine, molecular iodine and ultrafine particles in a coastal environment, Atmos. Chem. Phys.,11, 2545-2555, doi: 10.5194/acp-11-2545-2011, 2011.

Martín, J.C., Gómez, Gálvez, O., Baeza-Romero, M.T., Ingham, T., Plane, J.M.C., Blitz, M.A.: On the mechanism of iodine oxide particle formation, Phys. Chem. Chem. Phys., 15, 15612-15622, doi:10.1039/c3cp51217g, 2013.

McFiggans, G., Bale, C. S. E., Ball, S. M., Beames, J. M., Bloss, W. J., Carpenter, L. J., Gallagher, M. W.: Iodine-mediated coastal particle formation: an overview of the Reactive Halogens in the Marine Boundary Layer (RHaMBLe) Roscoff coastal study, Atmos. Chem. Phys., 10,2975-2999, doi: 10.5194/acp-10-2975-2010, 2010.

Mcfiggans, G., Coe, H., Burgess, R., Allan, J., Cubison, M., Alfarra, M. R.: Physics Direct evidence for coastal iodine particles from Laminaria macroalgae – linkage to emissions of molecular iodine, Atmos. Chem. Phys., 4, 701-713, doi: 10.5194/acp-4-701-2004, 2004.

Nayar S. and Bott K.: Current status of global cultivated seaweed production and markets, World Aquaculture 45(2):32-37, 2014

O'Dowd, C. D., Kaarle, H., Jyrki, M., Minna, V., Pasi, A., Gerrit, D. L.: Coastal new particle formation: Environmental conditions and aerosol physicochemical characteristics during nucleation bursts, J. Geophys. Res-atmos., 107, PAR 12-11–PAR 12-17, doi:10.1029/2000JD000206, 2002.

O'Dowd,C.D., Jimenez, J.L., Bahreini, R.: Marine aerosol formation from biogenic iodine emissions, Nature, 417(6889):632-636, doi: 10.1038/nature00775, 2002.

O'Dowd, C. D., De Leeuw, G.: Marine aerosol production: a review of the current knowledge, Philos. T R Soc. A., 365, 1753-1774, doi:10.1098/rsta.2007.2043, 2007.

Palmer, C.J., Anders, T.L., Carpenter, L.J., Küpper, F.C., Mcfiggans, G.B.: Iodine and halocarbon response of laminaria digitata to oxidative stress and links to atmospheric new particle production, Environ. Chem., 2, 282-290, doi:10.1071/EN05078, 2005.

Pechtl, S., Schmitz, G., von Glasow, R.: Modelling iodide–iodate speciation in atmospheric aerosol: Contributions of inorganic and organic iodine chemistry, Atmos. Chem. Phys., 7, 1381-1393, doi:10.5194/acp-7-1381-2007, 2007.

Redeker, K.R., Wang, N., Low, J.C., Mcmillan, A., Tyler, S.C., Cicerone, R.J.: Emissions of methyl halides and methane from rice paddies, Science, 290, 966-969, doi:10.1126/science.290.5493.966, 2000.

Roscoe, H. K., Jones, A. E., Brough, N., Weller, R., Saiz-Lopez, A., Mahajan, A. S., Schoenhardt, A., Burrows, J. P., and Fleming, Z. L.: Particles and iodine compounds in coastal Antarctica, J. Geophys. Res.-Atmos., 120, 7144-7156, doi:10.1002/2015JD023301, 2015.

Saiz-Lopez, A., Plane, J.M., Baker, A.R., Carpenter, L.J., Von, G.R., Mart ń, J.C., Mcfiggans, G., Saunders, R.W.: Atmospheric chemistry of iodine, Chem. Rev., 112, 1773-1804, doi:10.1021/cr200 029u, 2012a.

Saunders, R. W., Kumar, R., Gomez Martin, J. C., Mahajan, A. S., Murray, B. J., and Plane, J. M. C.: Studies of the Formation and Growth of Aerosol from Molecular Iodine Precursor, Zeitschrift Fur Physikalische Chemie-International Journal of Research in Physical Chemistry & Chemical Physics, 224, 1095-1117, 10.1524/zpch.2010.6143, 2010.

Sellegri, K., Yoon, Y.J., Jennings, S.G., O'Dowd, C. D., Pirjola, L., Cautenet, S.: Quantification of coastal new ultra-fine particles formation from in situ and chamber measurements during the BIOFLUX campaign, Environ. Chem., 2, 260-270, doi:10.1071/EN05074, 2006.

Seto, F.Y.B., Duce, R.A.: A laboratory study of iodine enrichment on atmospheric sea-salt particles produced by bubbles, J Geophy. Res., 77, 5339-5349 , doi:10.1029/JC077i027p05339, 1972.

Shah, M., Wuilloud, R.G., Kannamkumarath, S.S., Caruso, J.A.: Iodine speciation studies in commercially available seaweed by coupling different chromatographic techniques with UV and ICP-MS detection, J Anal. Atom. Spectrom., 20, 176-182, doi:10.1039/b415756g, 2005.

Sipilä, M., Sarnela, N., Jokinen, T., Henschel, H., Junninen, H., Kontkanen, J., Richters, S., Kangasluoma, J., Franchin, A., Peräkylä, O.: Molecular-scale evidence of aerosol particle formation via sequential addition of HIO3, Nature, 537, 532, doi:10.1038/nature19314, 2016.

Sive, B.C., Varner, R.K., Mao, H., Blake, D.R., Wingenter, O.W., Talbot, R.: A large terrestrial source of methyl iodide, Geophy. Res. Lett., 34, 251-270 , doi:10.1029/2007gl030528, 2007.

Wang, K.E., Jiang, S.J.: Determination of iodine and bromine compounds by ion chromatography /dynamic reaction cell inductively coupled plasma mass spectrometry, Anal. Sci., 24, 509-514 , doi:10.2116/analsci.24.509, 2008.

Wei, L., Hongxia, Y., Bing, L., Dengyun, C., Huijuan, Z.: Speciation Stabilities of Iodine in underground Water by High Performance Liquid Chromatography-Inductively Coupled Plasma Mass Spectrometry, Chinese J of Anal. Chem., 35, 571-573, doi: 10.1016/s1872-2040(07)60047-4, 2007.

Wimschneider, A., Heumann, K.G.: Iodine speciation in size fractionated atmospheric particles by isotope dilution mass spectrometry, Fresen. J Anal. Chem., 353, 191-196, doi:10.1007/BF00322957, 1995.

Xu, S., Xie, Z., Li, B., Liu, W., Sun, L., Kang, H., Yang, H., Zhang, P.: Iodine speciation in marine aerosols along a 15 000-km round-trip cruise path from Shanghai, China, to the Arctic Ocean, Enviro. Chem., 7, 406-412, doi: 10.1071/EN10048, 2010.

Yang, Y., Peng, Y., Chang, Q., Dan, C., Guo, W., Wang, Y.: Selective Identification of Organic Iodine Compounds Using Liquid Chromatography-High Resolution Mass Spectrometry, Anal. Chem.,88, 1275, doi: 10.1021/acs.analchem.5b03694, 2016.

Yoon, Y. J., O'Dowd, C. D., Jennings, S. G., Lee, S. H.: Statistical characteristics and predictability of particle formation events at Mace Head, J Geophy. Res.111,doi:10.1029/2005JD00 6284, 2006.

Yoshida, S., Muramatsu, Y., Katou, S., Sekimoto, H.: Determination of the chemical forms of iodine with

IC-ICP-MS and its application to environmental samples, J Radioanal. Nucl. Chem., 273, 211-214, doi:10.1007/s10967-007-0738-4, 2007.

Yu, H. , Zhou, L., Dai, L., Shen, W., Dai, W., Zheng, J.: Nucleation and growth of sub-3 nm particles in the polluted urban atmosphere of a megacity in China, Atmos. Chem. Phys., 16, 18653-18690, doi:10.5194/acp-16-2641-2016, 2016.

Yu, H., Wu, C., Wu, D., Yu, J. Z.: Size Distributions of Elemental Carbon and its Contribution to Light Extinction in Urban and Rural Locations in the Pearl River Delta region, China, Atmos. Chem. Phys., 10: 5107-5119, doi:10.5194/acp-10-5107-2010, 2010.

Yun, L., Peng, Y., Chang, Q., Zhu, Q., Guo, W., Wang, Y.: Identification of Organic Iodine Compounds and their Transformation Products in Edible Iodized Salt using Liquid Chromatography-High Resolution Mass Spectrometry, J Agr. Food Chem., 65, 5384-5389, doi:10.1021/acs.jafc.7b01759, 2017.

Zhang, X.: A picture of polar iodinated disinfection byproducts in drinking water by (UPLC/)ESI-tqMS, Environ. Sci. Technol.,43, 9287., doi:10.1021/es901821a, 2009.

Zhang, W., Liu, X., Jia, X., Yi, H., Liu, X., Xie, X., Lu, J., Duan, T., Chen, H.: Fast Speciation of Iodide and Iodate in Edible Salts and Human Urine by Short Column IC Coupled with Inductively Coupled Plasma MS, Chromatographia., 72, 1009-1012, doi:10.1365/s10337-010-1756-x, 2010.

Table 1. Organic iodine compounds that were detected at least once in the aerosol samples. n: the number of samples. Four $PM_{2.5}$ samples were collected at the inland site; three $PM_{2.5}$ samples and three sets of nano-MOUDI samples were collected at the coastal site. m/n numbers in right 4 columns: a given molecular formula was detected in m out of n samples. A blank cell means the formula was not detected in any samples. Also shown are measured ion mass, exact ion mass and the number of isomers based on the number of chromatographic peaks observed for given ion mass in the samples. Bold formulas are observed in ESI+ mode and others in ESI- mode.

Molecular formula	**Measured ion mass (Da)**	**exact ion mass (Da)**	**Isomer number**	**Coastal site (n=6)**			**Inland site (n=4)**	**All samples**
				I-NPF	**Continental NPF**	**Non-NPF**		
$C_2H_3O_2I$	184.9099	184.9099	1	3/4	1/1	1/1	4/4	9/10
$C_3H_3O_2I$	196.9098	196.9099	1	4/4	1/1		1/4	6/10
CH_2I_2	266.8177	266.8168	1	3/4	1/1		1/4	5/10
$C_2H_2O_2I_2$	310.8079	310.8066	1	4/4				4/10
$CH_2SO_3I_2$	346.7743	346.7736	1	2/4	1/1			3/10
$C_6H_4NO_4I$	279.9112	279.9107	1	3/4	1/1	1/1	4/4	9/10
$C_{10}H_6NO_3I$	313.9319	313.9314	1	4/4	1/1	1/1	3/4	9/10
$C_6H_4NO_3I$	263.9164	263.9158	1	4/4	1/1	1/1	2/4	8/10
$C_7H_6NO_4I$	293.9269	293.9263	2	3/4	1/1			4/10
C_5H_4NOI	221.9414	221.9416	2	3/4				3/10
C_6H_6NOI	235.9571	235.9572	2	3/4				3/10
C_7H_8NOI	249.9726	249.9729	3	3/4				3/10
$C_9H_{10}NO_4I$	321.9572	321.9576	2	1/4	1/1		1/4	3/10
$C_8H_6NO_5I$	321.9216	321.9212	1	2/4				2/10
C_9H_6NOI	271.9570	271.9572	2	2/4				2/10
$C_8H_8NO_5I$	323.9370	323.9369	1	1/4				1/10
$C_8H_7O_2I$	260.9411	260.9412	1	3/4	1/1	1/1	2/4	7/10
$C_7H_5O_4I$	278.9156	278.9154	2	2/4	1/1	1/1	2/4	6/10
$C_7H_5O_2I$	246.9260	246.9256	1	3/4	1/1		1/4	5/10
$C_8H_5O_3I$	274.9210	274.9205	1		1/1		2/4	3/10
$C_6H_3OI_3$	470.7245	470.7240	1	1/4	1/1			2/10
$C_7H_4O_3I_2$	388.8177	388.8172	1	1/4	1/1			2/10
$C_7H_5O_3I$	262.9209	262.9205	2	1/4	1/1			2/10
$C_7H_6O_2I_2$	374.8383	374.8379	1	1/4	1/1			2/10
$C_7H_7O_4I$	280.9298	280.9311	1	2/4				2/10
$C_8H_4O_2I_2$	372.8230	372.8222	1	1/4	1/1			2/10
$C_8H_6O_2I_2$	386.8382	386.8379	1	1/4	1/1			2/10
$C_8H_6O_3I_2$	402.8319	402.8328	1	1/4	1/1			2/10
$C_8H_7O_3I$	276.9361	276.9362	1	1/4	1/1			2/10
$C_8H_8O_3I_2$	404.8489	404.8485	1	2/4				2/10
$C_9H_7O_3I$	288.9372	288.9362	1	1/4				1/10
$C_9H_7O_4I$	304.9309	304.9311	2	1/4				1/10
$C_7H_{11}N_2I$	251.0044	251.0045	1	3/4			1/4	4/10
$C_8H_{11}N_6I$	319.0172	319.0168	1	1/4				1/10

$C_4H_4N_2I_2$	334.8547	334.8542	1	1/1	1/10

Table 2. Comparison of iodine species in $PM_{2.5}$ between the inland urban site and the coastal site. iodide: the sum of I^-, I_3^- and I^--metal complexes (if present). IO_x^-: the sum of IO_3^-, IO_2^- and IO^-; SOI: soluble organic iodine that is calculated as the difference between total iodine and the sum of iodide and IO_x^-. I-AA: the sum of iodoacetic acid and diiodoacetic acid; I-PA: iodopropenoic acid; I-MSA: iodomethanesulfonic acid;CHI_2^-: diiodomethane; I-aromatics: total aromatic iodine compounds; I^--organic adducts: iodide-organic adducts. Also shown are iodine species measured by IC-ICP-MS at Mace Head (Gilfedder et al., 2008), an Ireland coastal site, and Regensburg (Wimschneider and Heumann, 1995), an inland site of southern Germany. %: the percentages of iodine species in total iodine.

Iodine species	Inland site (n=4)		Coastal site (n=6)		Mace Head, Ireland		Regensburg, Germany	
	Conc. (pmol m^{-3})	%	Conc. (pmol m^{-3})	%	Conc. (pmol m^{-3})	%	Conc (pmol m^{-3})	%
iodide	1.0-3.7	23 ±9	3.8-74.1	31 ±14	0.3-58	3.7-30	3.1-7.2	12-31
IOx^-	ND-0.087	0.3 ±0.6	1.5-53.1	23 ±14	nd-15	0.1-7.2	12.6-54.2	69-88
SOI	5.4-7.5	77 ±9	14.2-66.1	46 ±27	3.7-509	69-96		
I^--organic adducts	4.3-6.1	64 ±8	6.7-62.9	31 ±16				
CH_2I^-	ND-0.083	0.2 ±0.4	0.036-0.74	0.4 ±0.7				
I-AA	0.054-0.25	1.6 ±1.0	0.57-2.2	4.8 ±5.6				
I-MSA	ND	0	ND-0.28	0.09±0.12				
I-PA	ND-0.016	0.04 ±0.07	0.16-5.2	5.9 ±4.6				
I-aromatics	0.76-1.2	12±3	0.1-12.3	6.7 ±6.8				
Total Iodine	6.5-11.2		19.5-122.6		10-532		15.7-61.3	

Figure 1. Locations of two sampling sites: ① the coastal site at Xiangshan Gulf ② the inland urban site that is 200 km from the coast. The blue color indicates the coastal area of China mainland.

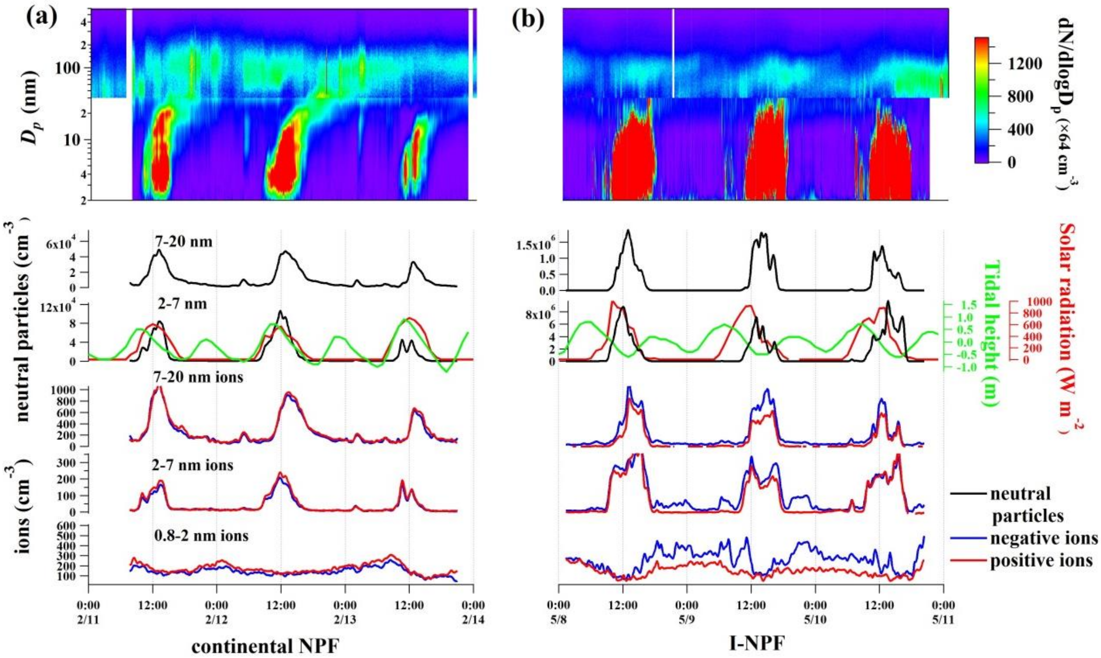

Figure 2. Particle number concentration during (a) the continental NPF days from February 11 to 13, 2018 and (b) the iodine-induced NPF (I-NPF) days from May 8 to 11, 2018. From top to bottom: particle size spectra of the NPF events; diurnal variations of 7-20 nm and 2-7 nm neutral particles (black curves); diurnal variations of 7-20 nm, 2-7 nm and 0.8-2 nm negative (blue curves) and positive ions (red curves). Solar radiation and tidal height were obtained from local maritime authority and plotted as red and green curves, respectively.

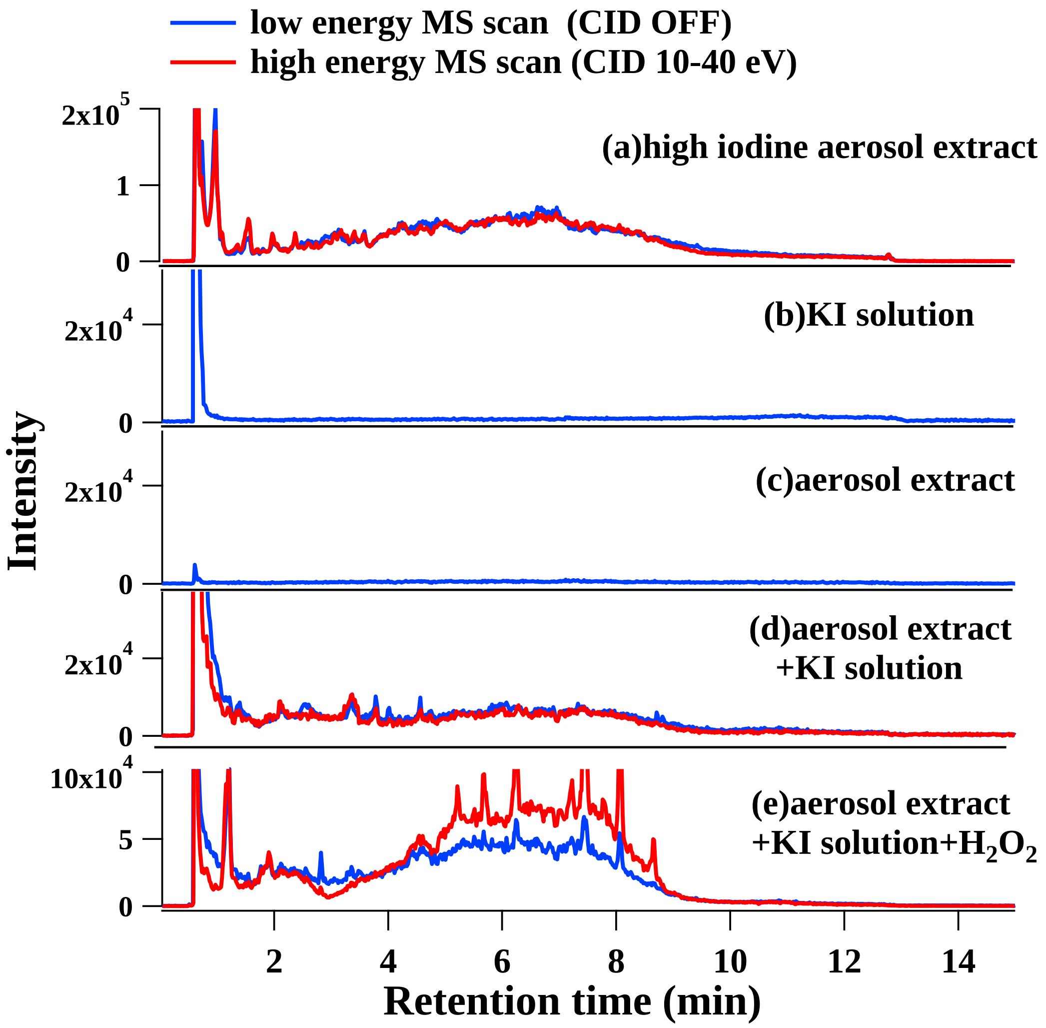

Figure 3. Ion chromatograms of m/z 126.9039 of (a) aerosol extract with high concentration of iodine, (b) pure potassium iodide (KI) solution (1 mmol L^{-1}), (c) aerosol extract with low concentration of iodine, (d) the KI solution mixed with the aerosol extract with low concentration of iodine and (e) The KI solution+aerosol extract mixture with the addition of 10 mmol L^{-1} H_2O_2 solution. Blue curves: low energy MS scan mode, in which collision induced dissociation is off and molecular ions are subject to in-source fragmentation only. Red curves: high energy MS scan mode, in which molecular ion are subject to both in-source fragmentation and 10-40 eV collision induced dissociation.

	Steps	MS method	Data acquired
1	MD *vs.* m/z diagram comparison between aerosol and aerosol+KI+H_2O_2/O_3	Low energy MS scan	m/z and RT of potential organic iodine ions
2	Elemental composition calculation Chemspider search	MSMS confirmation	80 possible CHONSI chemical formulas
3	Targeted screening in real aerosol samples based on m/z and RT	Low energy MS scan	35 formulas (47 organic iodine compounds) and their peak area observed in aerosol samples
4	4 compounds quantified with their standards; 43 compounds semi-quantified with surrogate standards	Low energy MS scan of commercial standards	Concentrations of individual non-aromatic compounds and total aromatic iodine compounds

Figure 4. Identification and semi-quantification steps of unknown organic iodine compounds in ambient aerosols

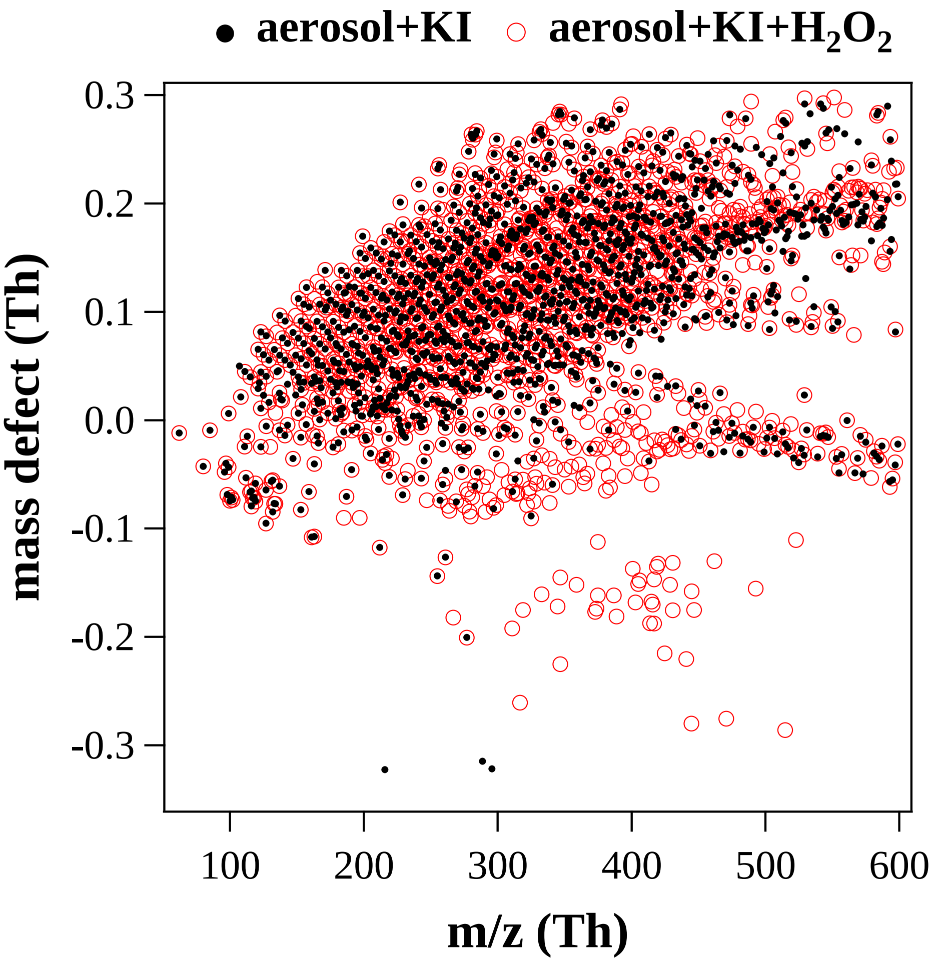

Figure 5. Mass defect (MD) *vs.* m/z diagram of molecular ions before (black dots) and after (red circles) the addition of H_2O_2 into aerosol extract+KI mixture. The mass spectrum of all ions above background level (10^4) was reconstructed by integrating over retention time 0-15 min.

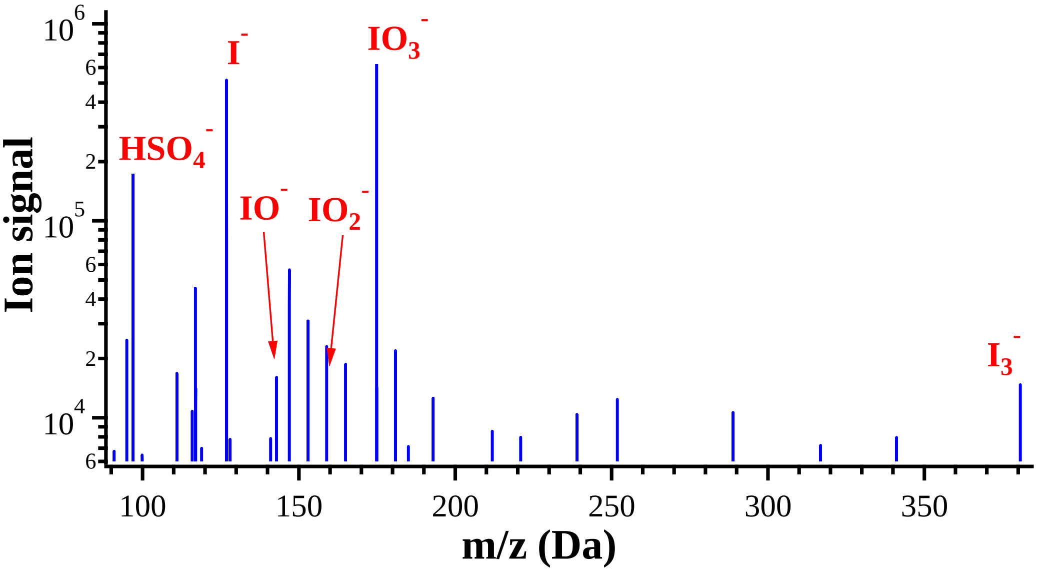

Figure 6. Integrated mass spectrum of molecular ions between retention time 0.5-0.7 min of an S13 nano-MOUDI sample (10-18 nm particles).

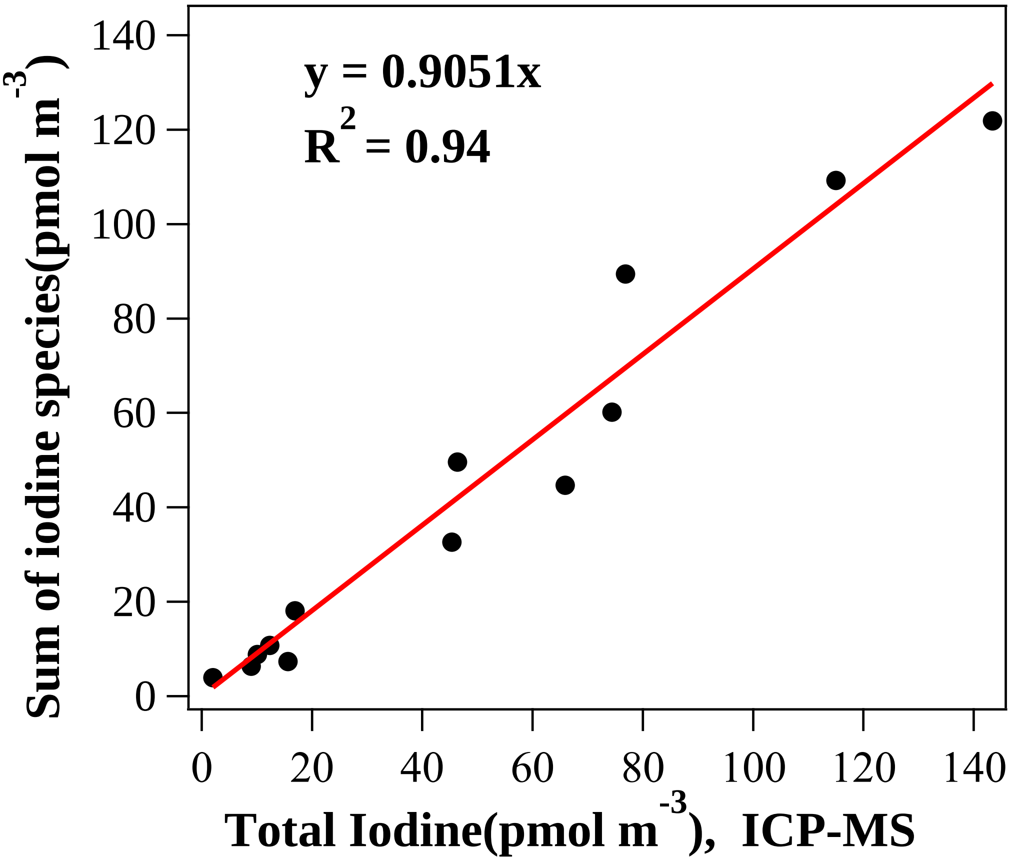

Figure 7. A comparison between the sum of all iodine species measured by our method and total iodine concentration measured by ICP-MS. Red line shows the linear regression between the two methods with a R^2 of 0.94.

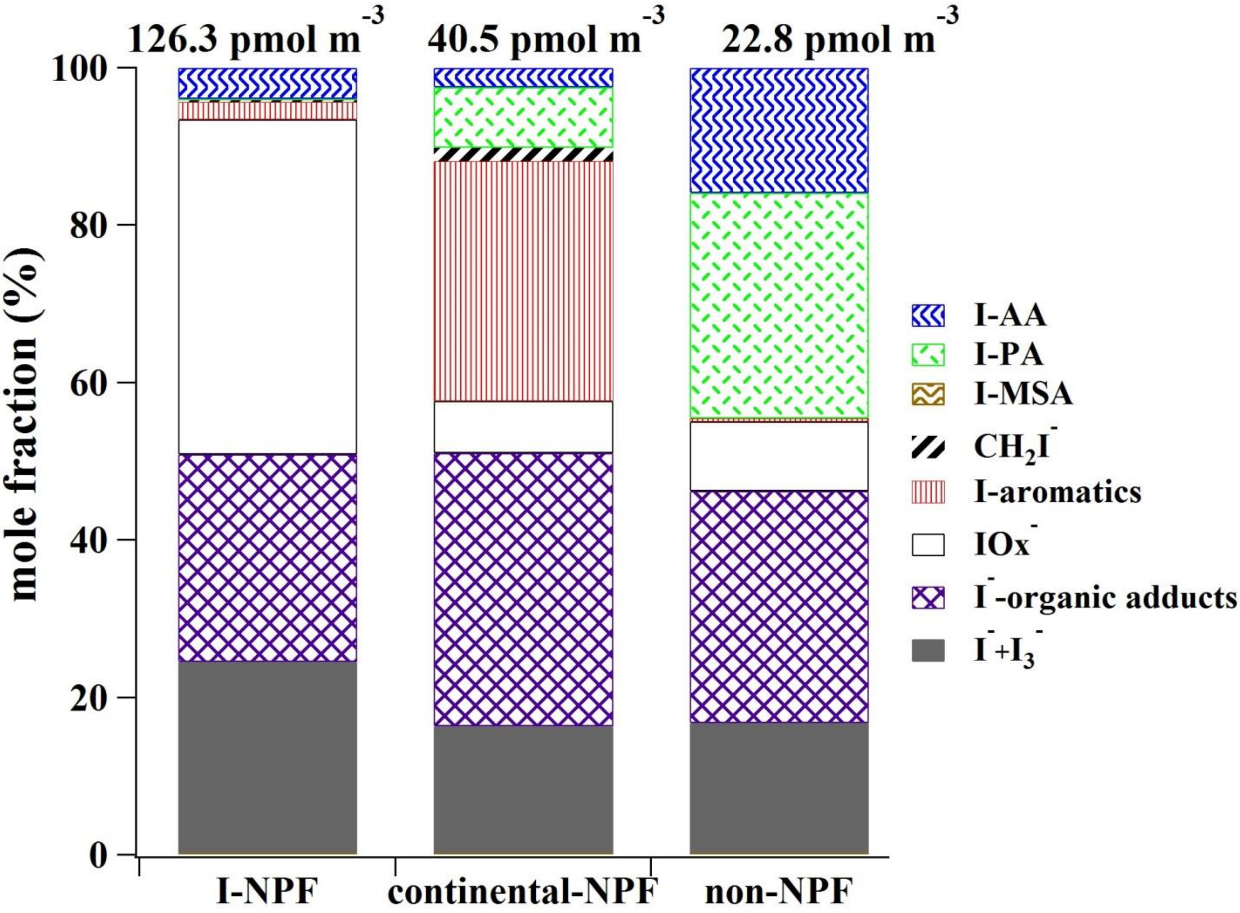

Figure 8. Total concentrations and mole fractions of iodine species in 10 nm-18 μm particles during the iodine-induced NPF (I-NPF), continental NPF and non-NPF days. I-AA: the sum of iodoacetic acid and diiodoacetic acid; I-PA: iodopropenoic acid; I-MSA: iodomethanesulfonic acid;CHI_2^-: diiodomethane; I-aromatics: total aromatic iodine compounds；IO_x^-: $[IO_3^-]+[IO_2^-]+[IO^-]$; I^--organic adducts：iodide-organic adducts； I^-＋I_3^-: the sum of iodide and triiodide.

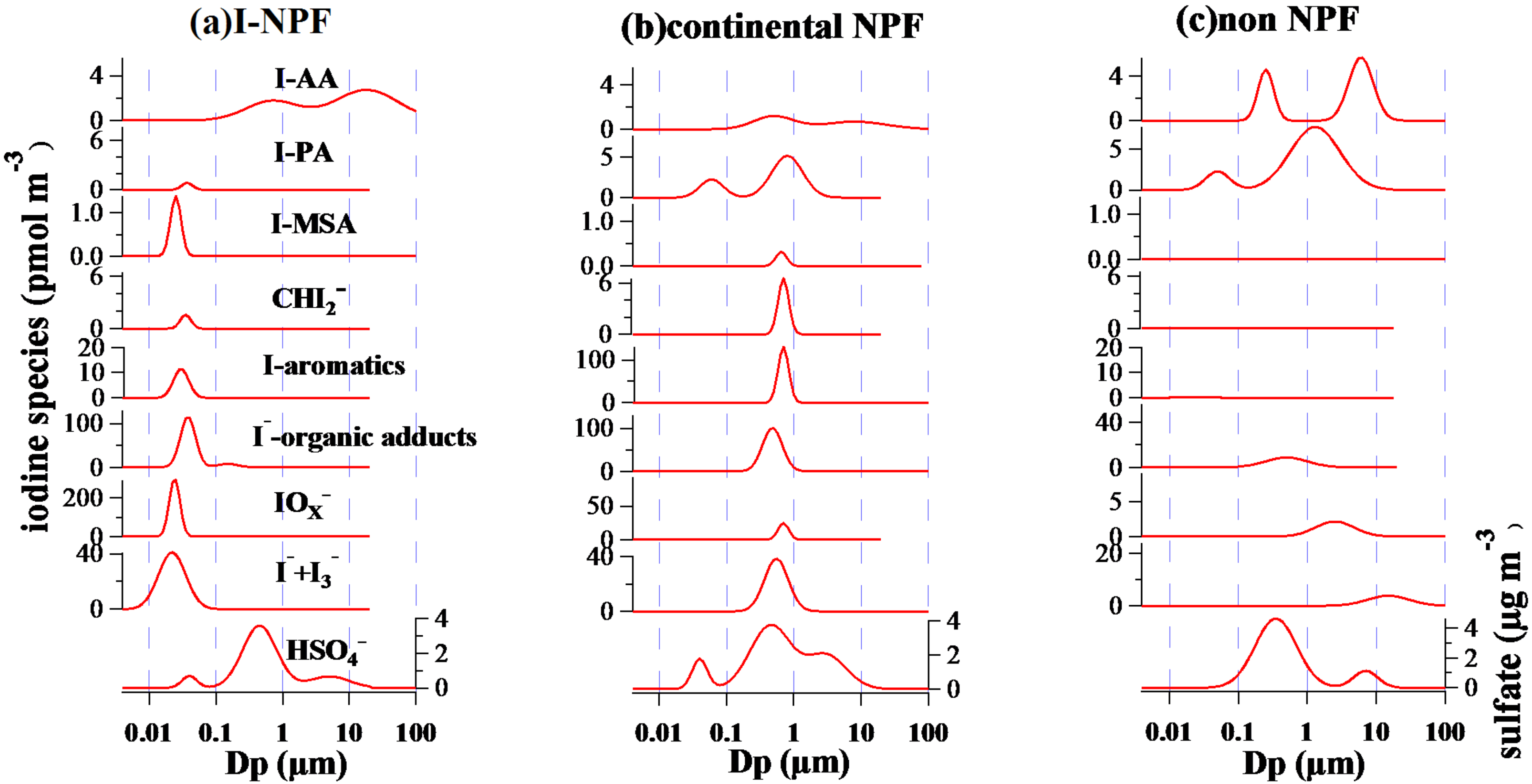

Figure 9. Mass size distribution of iodine species in 10 nm-18 μm particles during (a) iodine-induced NPF (I-NPF) days, (b) continental NPF days and (c) non-NPF days. Continuous size distributions of iodine species were inverted from the measured mass concentrations in the 13 size bins of nano-MOUDI. I-AA: the sum of iodoacetic acid and diiodoacetic acid; I-PA: iodopropenoic acid; I-MSA: iodomethanesulfonic acid;CHI_2^-: diiodomethane; I-aromatics: total aromatic iodine compounds； IO_x^-: $[IO_3^-]$+$[IO_2^-]$+$[IO^-]$; I^--organic adducts： iodide-organic adducts; I^-＋I_3^-: the sum of iodide and triiodide